# Nuclear assembly in giant unilamellar vesicles encapsulating *Xenopus* egg extract

Sho Takamori[1], Hisatoshi Mimura[1], Toshihisa Osaki[1], Tomo Kondo[2,†], Miyuki Shintomi[3], Keishi Shintomi[4], Miho Ohsugi[2,†], and Shoji Takeuchi[1,5,6]

[1]Artificial Cell Membrane Systems Group, Kanagawa Institute of Industrial Science and Technology, 3-2-1 Sakado, Takatsu-ku, Kawasaki, Kanagawa 213-0012, Japan.

[2]Department of Life Science, Graduate School of Arts and Sciences, The University of Tokyo, Meguro-ku, Tokyo 153-8902, Japan.

[3]Life Science Network , The University of Tokyo, Meguro-ku, Tokyo 153-8902, Japan.

[4]Chromosome Dynamics Laboratory, RIKEN, Wako, Saitama 351-0198, Japan.

[5]Institute of Industrial Science, The University of Tokyo, 4-6-1 Komaba, Meguro-ku, Tokyo 153-8505, Japan.

[6]Department of Mechano-Informatics, Graduate School of Information Science and Technology, The University of Tokyo, 7-3-1 Hongo, Bunkyo-ku, Tokyo 113-8656, Japan.

[†]Present address: Department of Biological Sciences, Graduate School of Science, The University of Tokyo, 7-3-1 Hongo, Bunkyo-ku, Tokyo 113-0033, Japan.

**Abstract**

The reconstitution of a cell nucleus in a lipid bilayer-enclosed synthetic cell makes great strides in bottom-up synthetic biology. In this study, we propose a method for assembling a nucleus in giant unilamellar vesicles (GUVs). To induce reconstitution of the nucleus, we utilise interphase egg extract of African clawed frogs *Xenopus laevis*, known as a biochemically controllable cell-free system capable of transforming an added sperm chromatin into a nucleus *in vitro*. We enhanced GUV-formation efficiency by the inverted emulsion method through incorporating prolonged waiting time and adding chloroform into lipid-dispersed oil, facilitating subsequent nuclear assembly reactions in the GUVs. Characterisation of nucleus-like structures formed in the GUVs revealed the presence of dense DNA and accumulated GFP-NLS in the structure, indicative of functional nuclear import. Immunostaining further validated the presence of nuclear pore complexes on the surfaces of these nucleus-like structures. Moreover, we observed a positive correlation between sizes of GUV and nucleus-like structure/nucleus. Our approach provides insights into nuclear assembly in lipid bilayer-enclosed cell-like confinement and becomes a platform for constructing artificial cellular systems that closely mimic eukaryotic cells.

## Introduction

Cell nucleus serves as a crucial subcellular compartment in eukaryotic cells, responsible for overseeing the maintenance of genetic materials and orchestrating their functions. Recent advancements in bottom-up synthetic biology have focused on constructing or integrating cell-like functional subcellular compartments in synthetic cells [1-5]. These efforts aim to replicate the functions of natural subcellular compartments such as photosynthesis in chloroplasts [6-8], mitochondrial respiration [9-11], and spatial organisation of gene expression reactions in the nucleus [12-13]. Among various eukaryotic subcellular compartments, the nucleus stands out as a central element in the regulation of eukaryotic cellular processes. Constructing the nucleus in synthetic cells encapsulated with a lipid bilayer represents a significant stride towards developing artificial eukaryotic cellular structures [14]. Reconstitution of natural cell nucleus has previously been achieved in bulk solution [15-17], microfluidic devices [18,19], and water-in-oil emulsions [20-22], by utilising egg extracts of the African clawed frog *Xenopus laevis*. The 'interphase' egg extract of *Xenopus laevis* is known as a biochemically manipulable cell-free system, capable of transforming sperm chromatin into a nucleus *in vitro* [15-17]. However, the challenge of assembling the nucleus in a lipid bilayer-enclosed confinement remains unmet. While encapsulation of an unspecified type of the egg extract into lipid bilayer-enclosed confinement has previously been reported [23], the typical yield in encapsulation of the interphase egg extract is low. This low yield can be attributed to the reported destabilisation of the lipid bilayer in the presence of *Xenopus* egg extract [24], highlighting the challenge of achieving stability in the lipid membrane surrounding the egg extract. Thus, stabilising the lipid bilayer could significantly improve the efficiency of encapsulation and enable the reconstitution of a nucleus in cell-like confinement enclosed with a lipid membrane.

69 In this study, we reconstitute a cell nucleus in giant unilamellar vesicles (GUVs). To accomplish the
70 assembly of a nucleus in GUVs, we confine interphase egg extract of *Xenopus laevis* supplemented
71 with *Xenopus* sperm chromatin by the inverted emulsion method. We incorporate an extended waiting
72 time as a parameter to enhance GUV yield, based on the finding that the formation of a lipid monolayer
73 at the oil-water interface, a crucial step in the inverted emulsion method, often requires a prolonged
74 period [25]. Additionally, we introduce chloroform into our lipid-dispersed oil, following reported
75 procedures that involve adding organic solvents to promote GUV formation by aggregating lipids and
76 improving their adsorption rate at the oil-water interface [26]. Using GUVs formed by encapsulating
77 the interphase egg extract, we induce nuclear assembly reactions in the GUVs. To confirm nuclear
78 reconstitution, we first identify the functionality of the nuclear membrane by a nuclear import assay.
79 Then, we conduct molecular confirmation of the nuclear membrane by immunostaining, and
80 quantitatively characterise the nuclear assembly events and geometric features of the formed GUVs
81 and nuclei.

82

83 **Results**

84 **Formation of GUVs encapsulating *Xenopus* egg extract**

85 To improve the encapsulation of *Xenopus* interphase egg extract (see 'Methods' for details on the
86 preparation of *Xenopus* interphase egg extract and sperm chromatin) into GUVs by the inverted
87 emulsion method, we assessed the impact of implemented waiting time ($\tau$: duration of waiting time; $\tau$
88 = 0/60/120 min) and added chloroform ($\Delta$: relative volume of added chloroform to the lipid-dispersed
89 oil; $\Delta$ = 0/5/10%) (Fig. 1; see 'Methods' for details on the intra-GUV nuclear assembly protocol).
90 Representative confocal micrographs of the formed GUVs are shown in Fig. 2a. At $\tau$ = 0 min and $\Delta$ =
91 0%, we observed that the number and size of GUVs encapsulating the egg extract were notably small,
92 unlike the GUVs encapsulating a typical dilute aqueous solution shown in Supplementary Fig. 1.

93 Meanwhile, we found an increasing trend in the number of GUVs encapsulating the egg extract with
94 prolonged waiting time and higher volumes of added chloroform. These observations suggest that
95 GUV-formation via the inverted emulsion method can be enhanced by implementing prolonged
96 waiting time and adding chloroform to lipid-dispersed oil.

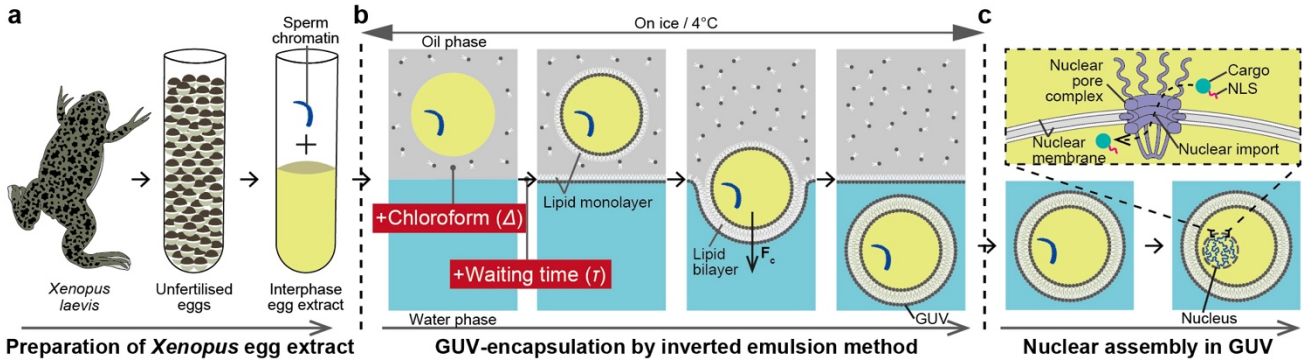


**Fig. 1: Three-step protocol for the assembly of a cell nucleus in GUVs.**

**a** Preparation of *Xenopus* interphase egg extract. Sperm chromatin is added to the egg extract prior to encapsulation into GUVs. **b** Encapsulation of sperm chromatin-added interphase egg extract into GUVs by the inverted emulsion method. Lipid monolayers are formed at the interfaces between water and oil phases. The formation of a lipid monolayer at the interfaces is enhanced by incubating the interfaces for the duration of the waiting time ($\tau$) and adding chloroform in a volume ($\Delta$) into lipid-dispersed oil. Centrifugal force ($F_c$) allows the egg extract emulsions surrounded by a lipid monolayer to pass through a lipid monolayer formed at the interface between the oil phase and the outside water phase, transforming them into GUVs. **c** Induction of nuclear assembly reactions in GUVs by incubation at 22/23°C for 90 min.

97

98

99

100

To evaluate the impact of implemented waiting time and added chloroform on i) the number of GUVs formed, ii) the encapsulation of *Xenopus* interphase egg extract, and iii) the diameter of GUVs produced by the inverted emulsion method, we performed image segmentation of GUVs and computed these parameters from the micrographs (see 'Methods' for details on the image segmentation and computation of parameters). The number of GUVs plotted in Fig. 2b exhibited consistent increases with higher volumes of added chloroform (e.g., from 119 GUVs to 857 GUVs at $\tau$ = 120 min), while the relationship between the number of GUVs and increased waiting time was less consistent (Supplementary Fig. 2). Similarly, we observed a consistent rise of the proportion of GUVs encapsulating the GFP-dispersed egg extract with higher volumes of added chloroform (e.g., from ~38% to ~77% at $\tau$ = 120 min), as shown in Fig. 2c, with no significant change observed in relation to prolonged waiting time (Supplementary Fig. 3). Raw values of mean GFP intensity in the GUV lumen and background used for computing the parameters in Fig. 2c and Supplementary Fig. 3 are shown in Supplementary Fig. 4. Next, the violin plot of GUV diameter revealed that the majority of GUVs had diameters below 5 μm, as seen in Fig. 2d. The number of GUVs larger than 5 μm notably increased with higher volumes of added chloroform, as depicted in Fig. 2e, whereas only a slight increase was observed with increased waiting time (Supplementary Fig. 5). We did not see significant changes in the proportion of GUVs whose diameter was larger than 5 μm in GUVs formed under each condition, in relation to both waiting time and chloroform (Supplementary Fig. 6). These results suggest that the implementation of prolonged waiting time and the addition of chloroform increase i) the number of GUVs formed by the inverted emulsion method, ii) the proportion of GUVs encapsulating the egg extract in the observed GUVs, and iii) the number of relatively large GUVs in the population, although statistically significant improvements in these parameters were primarily associated with increased chloroform volume.

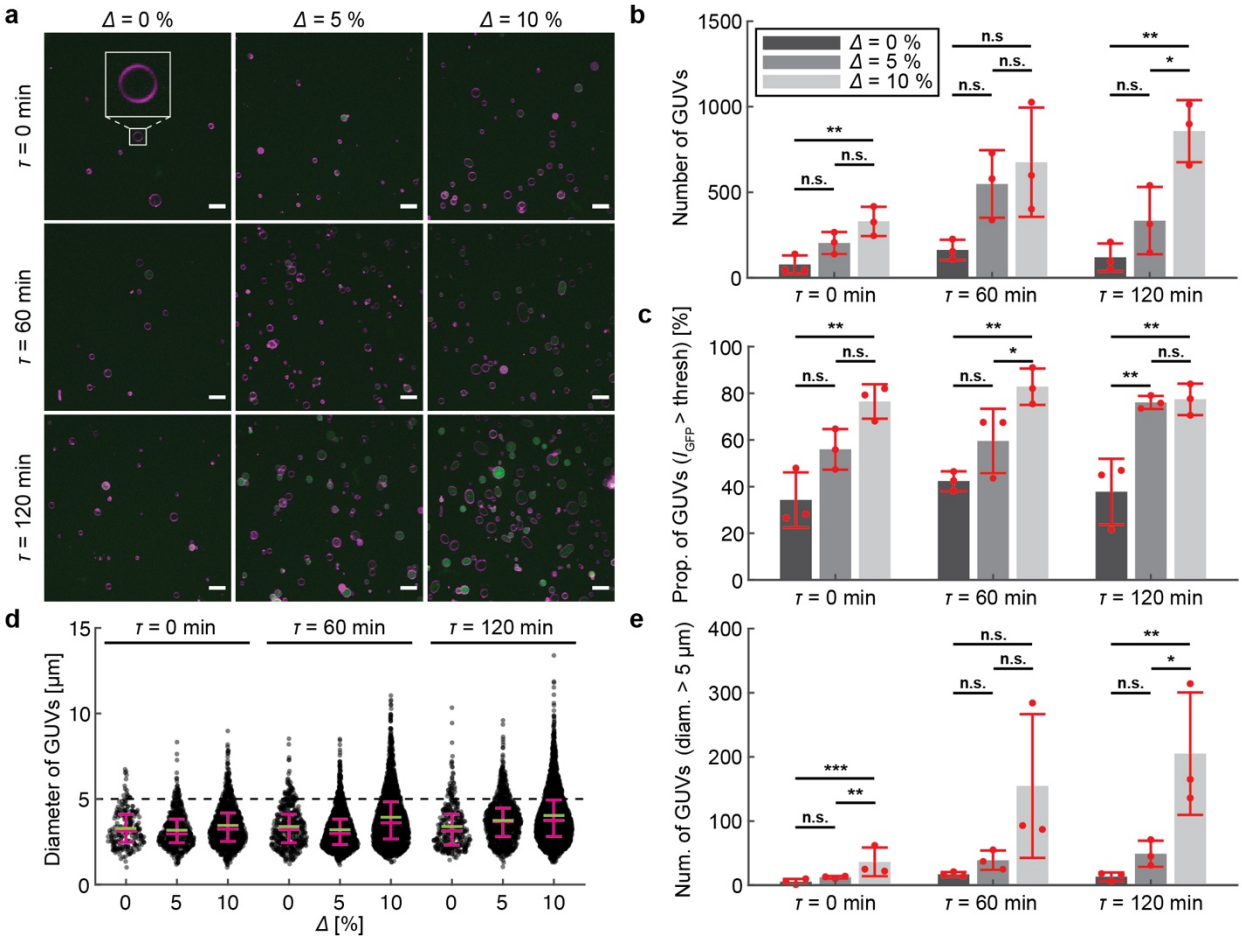


**Fig. 2: Formation of GUVs encapsulating *Xenopus* interphase egg extract.**

**a** Representative micrographs of GUVs encapsulating the sperm chromatin-added interphase egg extract formed by the inverted emulsion method. $\tau$ denotes duration of waiting time and $\Delta$ denotes added volume of chloroform to the lipid-dispersed oil. Magenta is lipid membrane (RhPE) and green is GFP dispersed in the egg extract. An inset enclosed within a white box depicts a zoom-in of a typical GUV formed at $\tau = 0$ min and $\Delta = 0\%$. Scale bar: 10 μm. **b** The number of GUVs found (10 micrographs per plot, $N = 3$). **c** Proportion of GUVs with mean GFP intensity higher than the computed threshold in the observed GUVs (10 micrographs per plot, $N = 3$). **d** The diameter of GUVs (sum of $N = 3$ with 10 micrographs per each). **e** The number of GUVs with diameter larger than 5 μm (10 micrographs per plot, $N = 3$). In panels b-c and e, one-way ANOVA followed by a *post-hoc* Tukey-Kramer multiple comparison test was performed. See 'Methods' for the details on statistical analysis and Supplementary Tables 1-3 for the summary of statistics.

126

127 **Formation of nucleus-like structures in GUVs**

128 To initiate nuclear assembly reactions in GUVs encapsulating sperm chromatin-added *Xenopus*
129 interphase egg extract, GUVs formed under various waiting time and chloroform conditions were
130 incubated at 22ºC (or 23ºC) for 90 min. A nuclear import assay utilising GFP fused with a nuclear
131 localisation signal derived from simian vacuolating virus 40 (GFP-NLS; see 'Methods' for details on
132 the preparation of GFP-NLS).) was conducted as the primary means of identifying nucleus assembly,
133 following established protocols in water-in-oil emulsions [20-22]. In this assay, GFP-NLS is expected
134 to be transported into the nucleus if a functional nuclear membrane with nuclear pore complexes is
135 assembled on the surface as illustrated in Fig. 1c, while passive dispersion of GFP without the NLS-
136 peptide is anticipated in the GUV lumen. Hereafter, the former condition is denoted as 'NLS(+)', and
137 the latter as 'NLS(-)'. Representative micrographs of these GUVs in the top row of Fig. 3a and
138 Supplementary Fig. 7 demonstrated that GFP clearly accumulated at the same location in the GUVs
139 under the NLS(+) condition, suggesting active nuclear import of GFP-NLS into the assembled nucleus.
140 In contrast, GFP was homogeneously dispersed in the GUVs containing dense DNA under the NLS(-)
141 condition, albeit with a slight accumulation of GFP lacking the NLS-peptide at the same location as
142 dense DNA observed in several confocal micrographs of GUVs in NLS(-) samples (Supplementary
143 Fig. 8). These confocal micrographs indicate successful assembly of nucleus-like structures in GUVs.

144

145 **Immunostaining of nuclear pore complexes on nuclear membrane**

146 To verify the presence of a nuclear membrane on the surface of nucleus-like structures formed in GUVs
147 (top row of Fig. 3a and Supplementary Fig. 7), we conducted immunostaining of nuclear pore
148 complexes (NPCs) using NPC antibodies (mAb414) [27,28]. GUVs containing a nucleus-like structure
149 were fixed with 2.0% glutaraldehyde and stained with mAb414-Alexa Fluor 594 (mAb414-AF594;
150 see 'Methods' for the details on immunostaining). Confocal micrographs of the GUVs are shown in

151 the top row of Fig. 3b and Supplementary Fig. 9. As a positive control experiment, we conducted
152 immunostaining of nuclei formed in the bulk form of sperm chromatin-added *Xenopus* interphase egg
153 extract using the same procedure, as depicted in the bottom row of Fig. 3b and Supplementary Fig. 10.
154 These confocal micrographs confirmed accumulations of mAb414-AF594 signals at the periphery of
155 nucleus-like structures in the GUVs, as well as at the periphery of nuclei formed in the bulk extract.
156 Manual inspection of the micrographs revealed that more than 15% of nucleus-like structures showed
157 the presence of NPCs on their surfaces (28 nucleus-like structures among the 169 structures fixed,
158 immunostained, and inspected in total). The rest of nucleus-like structures exhibited overstaining of
159 their interior by mAb414-AF594 (Supplementary Fig. 11). These immunostaining results indicate the
160 presence of a nuclear membrane on the surfaces of a certain number of nucleus-like structures observed,
161 thus confirming the successful reconstitution of the nucleus in the GUVs.

162

163

164

165

166

167

168

169

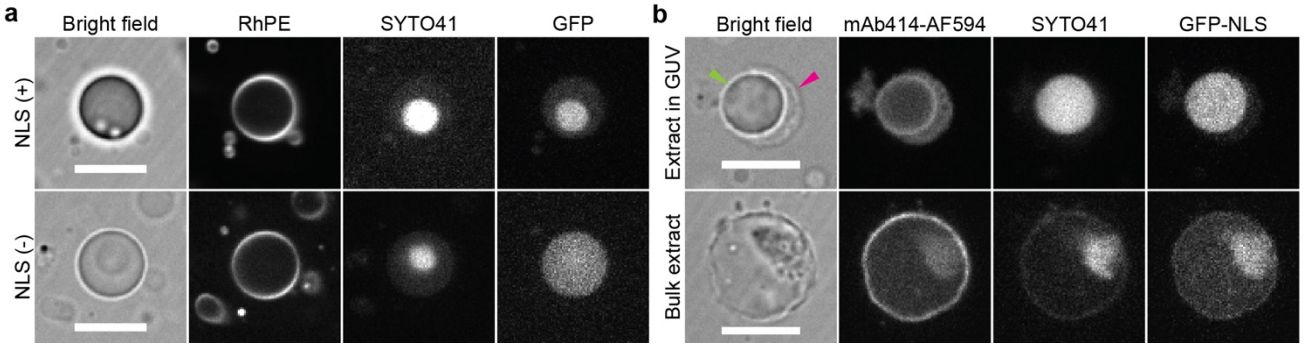


**Fig. 3: Formation of nucleus-like structures in GUVs and immunostaining of nuclear pore complexes.**

**a** GUVs after incubation for nuclear assembly reactions. RhPE: Lipid membrane, SYTO 41: nucleic acids (mainly DNA) stain. NLS(+): GFP with attached nuclear localisation signals (NLS); NLS(-): GFP without NLS peptide. See Supplementary Figs. 7-8 for additional examples. **b** A GUV containing a nucleus-like structure fixed with 2% glutaraldehyde and immunostained with mAb414-AF594 (top), and a nucleus formed under bulk condition, fixed and immunostained similarly (bottom). Arrow heads indicate GUV membrane (magenta) and nucleus-like structure (green). See Supplementary Figs. 9-10 for additional examples. Scale bar: 10 µm.

170

171

172

173

174

175

176

177

178 **Quantitative characterisation of nucleus-like structures in GUVs**

179 To characterise nucleus-like structures containing DNA and GFP-NLS accumulated through nuclear
180 import (top row of Fig. 3a and Supplementary Fig. 7), we analysed fluorescence in GUVs formed
181 under each of NLS(+) and NLS(-) conditions and incubated for nuclear assembly reactions. We first
182 defined C1 and C2 compartments in GUVs containing a nucleus-like structure carrying dense DNA
183 (Fig. 4a) and extracted the mean fluorescence intensity in C1 and C2 compartments (Supplementary
184 Fig. 12). We then computed the ratio of the fluorescence intensity (Fig. 4b-c). The violin plot of SYTO
185 41 intensity ratio showed similar distributions and mean values of approximately 2.3 under both
186 NLS(+) and NLS(-) conditions, in Fig. 4b (See Supplementary Table 4 for statistics). In contrast, the
187 distributions of GFP intensity ratio appeared significantly different ($p < 0.01$) between the two
188 conditions (see Supplementary Table 5 for statistics), with mean values of approximately 1.6 for
189 NLS(+) and 1.2 for NLS(-), as seen in Fig. 4c. These results suggest: 1) the presence of dense DNA in
190 the C1 compartment, and 2) significantly higher accumulation of GFP-NLS in the C1 compartment
191 under NLS(+) condition than NLS(-) condition.

192

193 To evaluate the impact of waiting time and chloroform addition on the formation of nucleus-like
194 structures in GUVs, we quantified structures containing both dense DNA and accumulated GFP-NLS.
195 'Nucleus-like compartments' (NLCs) were defined as C1 compartments having significantly higher
196 GFP intensity than C2 compartments, determined by a threshold GFP intensity ratio of ~1.5 (Fig. 4c;
197 see 'Methods' for the details on the definition and identification of NLCs). Successful formation of
198 NLC-containing GUVs occurred when both waiting time and chloroform volume were non-zero (Fig.
199 4d). Increasing chloroform volume proportionally increased the number of NLC-containing GUVs
200 under both $\tau$ = 60 and 120 min conditions. Extension of waiting time did not significantly affect the
201 proportion of NLC-containing GUVs (Supplementary Fig. 13). At $\tau$ = 120 min and $\Delta$ = 10%,

approximately 1.4% of the GUVs contained an NLC. These results indicate that prolonged waiting time and chloroform addition promote the formation of NLCs in GUVs, especially with higher chloroform volumes.

To assess the impact of the GUV size on the successful formation of NLCs and nuclei confirmed by immunostaining, we calculated the diameter of GUVs observed under the condition of $\tau$ = 120 min and $\Delta$ = 10%. The resulting violin plot showed a statistically significant difference ($p < 0.001$) between all combinations of GUVs containing an NLC, GUVs without NLC, and GUVs containing a nucleus (see Supplementary Table 7 for statistics) as plotted in Fig. 4e. The mean diameter of GUVs containing an NLC was 6.4 μm, that of GUVs without NLC was 5.0 μm, and that of GUVs containing a nucleus was 10.2 μm as indicated with green bars in Fig. 4e. In addition, we plotted the diameters of GUVs containing an NLC (grey dots) and a nucleus (magenta triangles) against observed diameters of NLCs and the nuclei and found a positive correlation between GUV volume and NLC and nucleus volume (correlation coefficient: $\rho \sim 0.93$, power law fit result: $y = 0.086\ x^{1.18}$), as shown in Fig. 4f. The corresponding NLC-to-GUV volume ratio and nucleus-to-GUV ratio were approximately 0.27 for NLCs and 0.25 for nuclei, as shown in Fig. 4g. These results suggest three points: 1) NLC formation and nucleus formation are more likely to occur in larger GUVs within the observed diameter range, 2) the size of NLCs and nuclei tends to increase with the size of GUVs within the observed volume range, and 3) the volume ratio between NLC and GUV and that between nucleus and GUV have similar distributions.

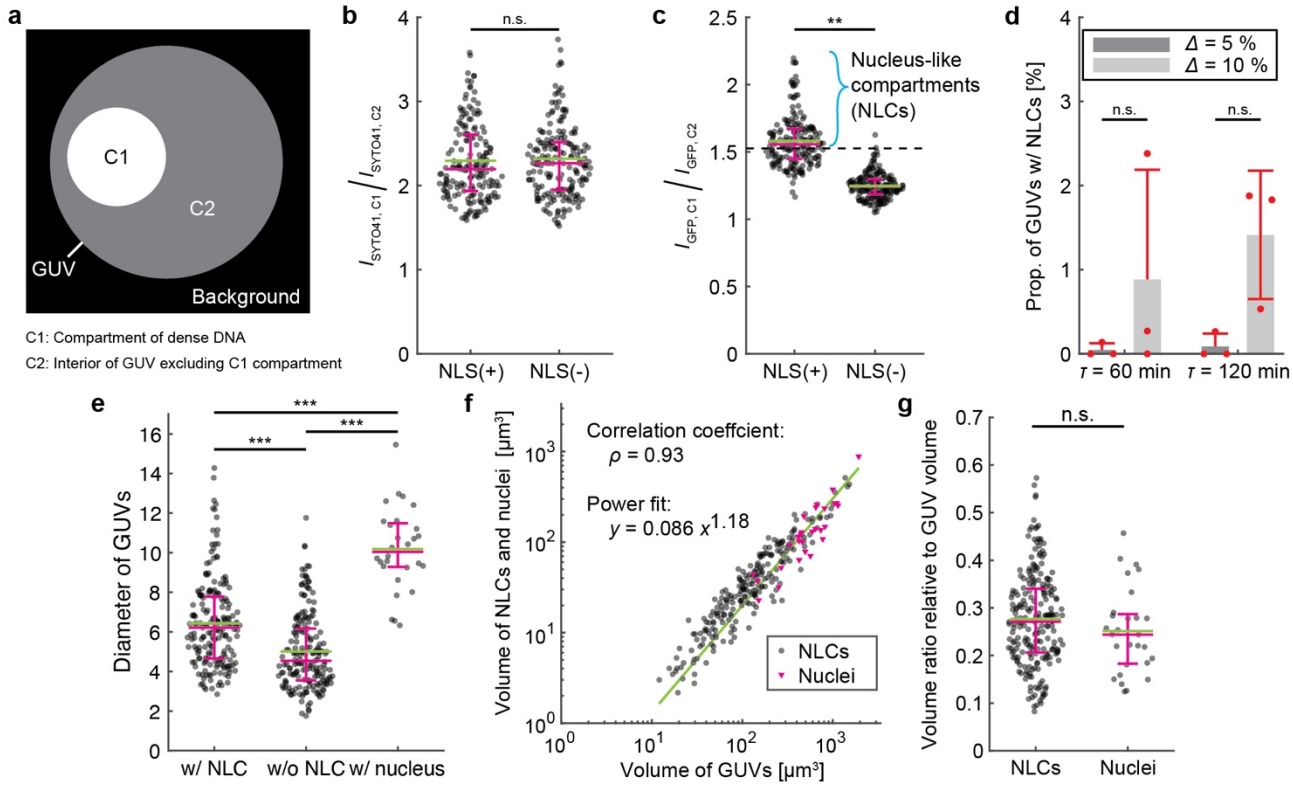


**Fig. 4: Quantitative analysis of NLCs and nuclei formed in GUVs.**

**a** Definition of internal compartments in a GUV. **b** Ratio of SYTO 41 intensity between C1 and C2 compartments in GUVs. $N = 182$ for NLS(+), $N = 193$ for NLS(-). **c** Ratio of GFP intensity between C1 and C2 compartments. The threshold of GFP-accumulation is mean + 3SD of NLS(-), indicated with a black dashed line (threshold value: 1.5). **d** Proportion of NLC-containing GUVs in the observed GUVs. Error bar denotes mean ± SD (partially omitted where the bar fell below zero). **e** Diameter of GUVs at $\tau = 120$ min and $\Delta = 10$ %. GUVs containing an NLC are denoted as 'w/ NLC', GUVs without NLC as 'w/o NLC', and GUVs containing a nucleus as 'w/ nucleus'. $N = 193$ for w/ NLC and w/o NLC, $N = 28$ for w/ nucleus. **f** Volumes of GUVs containing an NLC and that of NLCs are plotted with grey dots. Volumes of GUVs containing a nucleus are plotted in magenta triangles. The green line is a result of power fit ($y = 0.086\ x^{1.18}$). $N = 222$ for NLCs, $N = 28$ for nuclei. **g** Ratio of the volume of NLCs and nuclei to the volume of the GUVs. In panels b-c and e, magenta bars indicate the median ± quartile, while a green bar indicates the mean. In panels b-c and e, a two-sample t-test was performed. In panels d and g, Wilcoxon rank sum test was performed. In panel e, a Kruskal-Wallis test followed by *post-hoc* multiple comparisons using Bonferroni correction was performed. See 'Methods' for the details on statistical analysis and Supplementary Tables 4-8 for the summary of statistics.

## Discussion

In this study, we achieved the reconstitution of the cell nucleus in GUVs formed by the inverted emulsion method. Implementation of prolonged waiting time and addition of chloroform into lipid-dispersed oil improved the number of GUVs formed by the inverted emulsion method and the proportion of GUVs encapsulating sperm chromatin-added *Xenopus* interphase egg extract in the observed GUVs (Fig. 2). We found the formation of numerous nucleus-like structures in the GUVs demonstrating their nuclear import capability (Fig. 3a and Supplementary Fig. 7). Moreover, we confirmed the presence of nuclear pores on their surfaces (Fig. 3b), hence the presence of a nuclear membrane, by investigating through immunostaining of nuclear pore complexes. Furthermore, we identified an increase in the assembly frequency of nucleus-like compartments (NLCs), particularly along with an increase of added chloroform volume, as seen in Fig. 4d, and discovered a positive correlation between the size of GUVs and the size of internal NLCs and nuclei (Fig. 4f).

In our investigation, we noted that the implementation of waiting time and the addition of chloroform not only increased the number of GUVs encapsulating the egg extract but also enabled the formation of GUVs encapsulating a high concentration of the egg extract (Supplementary Fig. 4). We hypothesise that implemented waiting time and added chloroform in lipid-dispersed oil enhance the adsorption of lipid molecules at the oil-water interface and facilitate the formation of GUVs with more stable lipid membranes by the inverted emulsion method [25,26]. As a result, leakage of the encapsulated egg extract from the interior of the GUVs could have been reduced owing to the increased stability of the GUV-membrane, while the internal solution of GUVs formed by the inverted emulsion method normally experiences dilution of the internal content [29,30], as demonstrated in Supplementary Figs. 1 and 4. Provided that the probability of the nuclear assembly event decreases through the diminishment of required molecules by the extract leakage, the higher concentration of the egg extract

270 in GUVs could have contributed to the observed increase in NLC formation (Fig. 4d and
271 Supplementary Fig. 13).

272

273 In general, chloroform is deliberately eliminated from lipid-dispersed oil through evaporation as it is
274 widely considered harmful to biochemical reactions embedded in GUVs [30-32]. On the other hand,
275 recent investigations employing the inverted emulsion method have demonstrated successful induction
276 of gene expression reactions [29] and the bundle formation of cytoskeletal proteins [33-36] in GUVs
277 under conditions where chloroform was deliberately added into the lipid-dispersed oil. These studies
278 suggest that chloroform may have limited impact on biochemical reactions in GUVs, at least at the
279 concentrations utilised in these studies. Therefore, we adopted chloroform concentrations in our lipid-
280 dissolved oil ($\Delta$ = 5/10 %) consistent with those used in previous studies, leading to the formation of
281 the numerous egg extract-encapsulating GUVs (Fig. 2) and successful nuclear and NLC assembly in
282 the GUVs (Figs. 3, 4d-g and Supplementary Figs. 7, 9, 13).

283

284 The reconstitution of cell nuclei under micro-metre-scale three-dimensional confinement has
285 previously relied on water-in-oil emulsions, where the confirmation of assembled nuclei was achieved
286 only through a nuclear import assay [20-22]. In contrast, our approach involves encapsulating the egg
287 extract in a lipid bilayer of GUVs and reconstitutes a nucleus in the GUVs. The semi-permeability of
288 the lipid bilayer allowed the exchange of molecules between the inside and outside of the GUVs, while
289 essentially isolating the internal solution from the outer environment in confinement. This setup
290 enabled the characterisation of nucleus-like structures in an additional approach, similarly to previous
291 studies of *in vitro* nuclei formed in the bulk extract. We first identified the formation of nucleus-like
292 structures in GUVs by a nuclear import assay (Fig. 3a) and additionally conducted their molecular
293 characterisation through immunostaining (Fig. 3b). Our findings, indicating that only approximately

294 17% of NLCs carried nuclear pore complexes on their surfaces, highlight the significance of GUV
295 encapsulation in providing a more comprehensive understanding of *in vitro* nuclei formed under
296 confinement in GUVs.

297

298 We obtained several insights into size. First, we observed a significantly higher mean diameter of 10.2
299 μm for GUVs containing a nucleus, as shown in Fig. 4e, compared to the mean diameter of GUVs with
300 or without NLC. We consider that this discrepancy may be attributed to an unidentified effect of the
301 immunostaining procedure developed in this study but not necessarily a prerequisite for nuclear
302 assembly to occur. Furthermore, we confirmed a proportional relationship between the volume of
303 GUVs and that of NLCs and nuclei (Fig. 4f), where the evaluated power-law exponent fitted to 1.18.
304 This exponent is larger than the known exponents (0.7-0.9) between cell volume and nucleus volume
305 in various natural cells [37], resulting in a relatively higher nuclear-to-cytoplasmic (N/C) volume ratio
306 in these GUVs compared to many natural cells (Fig. 4g). We attribute this high N/C ratio to the large
307 volumes of sperm chromatin encapsulated in the GUVs. Additionally, we discovered that the size range
308 of GUVs containing an NLC and nucleus spanned approximately 1 to 16 μm, consistent with reported
309 dimensions of GUVs encapsulating *Xenopus* egg extract of unspecified types [24]. In contrast, we
310 confirmed the presence of larger emulsions in the lipid-dispersed oil just before the phase transfer
311 procedure in the inverted emulsion method (Supplementary Fig. 15). These observations might be
312 linked to instances of GUV rupture arising from the inverted emulsion method [31,38,39]. Lastly, we
313 found that a significant subset of the formed GUVs exhibited sizes smaller than the standard
314 dimensions of *Xenopus laevis* sperm chromatin (approximately 10 μm along the long axis), suggesting
315 the potential encapsulation of partial sperm chromatin fragments within the GUVs smaller than 10 μm.
316 Considering the broader applicability of the proposed protocol, it is anticipated that the protocol could
317 facilitate the complete encapsulation of arbitrarily long DNA molecules, including those at a genome-
318 scale. To achieve such encapsulation, it might be necessary to investigate methods for handling long

319 DNA molecules to prevent fragmentation due to physical forces or to develop techniques for sorting
320 GUVs to ensure the complete encapsulation of target DNA.

321

322 Taken together, this study has enabled the reconstitution of cell nuclei in GUVs, opening a range of
323 potential applications. Firstly, it may facilitate the investigation of the interaction between the cell
324 cortex and nuclear assembly [23], which has likely been hindered by the absence of cell cortex
325 anchoring proteins at the boundary of water-in-oil emulsions [40]. Moreover, the established protocol
326 holds promise for evolving into a method for transplanting artificial chromosomes into various
327 eukaryotic cells, integrating with artificial chromosome/genome technologies [41-44] and GUV-cell
328 fusion techniques [45,46]. For chromosome transplantation, further optimisation of lipid adsorption to
329 the oil-water interface and investigation into phase transfer conditions in the inverted emulsion method
330 might be necessary to form large GUVs encapsulating DNA of arbitrary size. Finally, we believe that
331 the reconstituted cell nuclei in GUVs will serve as a powerful tool for constructing artificial cellular
332 systems closely mimicking eukaryotic cells in bottom-up synthetic biology research.

333

334 **Methods**

335 **Preparation of interphase egg extract and sperm chromatin of the frog *Xenopus laevis***

336 Interphase egg extract was prepared as described previously [47] with modifications as follows: to
337 convert the cell cycle stage of the egg extract from mitosis into interphase, unfertilised eggs were
338 crushed using KMH (100 mM KCl, 2.5 mM $MgCl_2$, 20 mM HEPES-KOH at pH 7.7) containing 1 mM
339 $CaCl_2$ rather than a calcium-ionophore treatment; to completely separate the egg extract from insoluble
340 material (e.g., actin filaments and mitochondria), crude egg extract isolated by the initial centrifugation
341 was diluted in KMH (10% volume of the original extract), and then clarified by another round of
342 centrifugation at 45,000×g. Sperm chromatin was prepared as described previously [47]. In every

343 preparation of the egg extract and sperm chromatin, their quality was evaluated by monitoring nuclear
344 assembly in the bulk format (Fig. 3b and Supplementary Fig. 10) and in water-in-oil emulsions
345 (Supplementary Fig. 14) under a fluorescence microscope.

346

347 **Preparation of GFP-NLS**

348 GFP-NLS in Fig. 3 and Supplementary Figs. 1, 9-11, was prepared by following a standard protocol
349 [48]. GFP-NLS used in other sections of this paper was prepared by Dr. Yuki Hara by following a
350 similar standard protocol. Briefly, *Escherichia coli* BL21 (DE3) cells were transformed with a pGEX
351 vector containing a GFP-NLS gene. The cells were incubated in four 250 mL aliquots of LB medium
352 at 30°C with shaking at 250 RPM until $OD_{600}$ ~ 0.8. 1 mM IPTG was added, and the cultures were
353 further incubated for 5 h. The cells were harvested by centrifugation, and the pellets were stored at -
354 80°C until next day. On the following day, the frozen cell pellets were resuspended in PBS lysis buffer
355 (consisting of PBS pH 7.2 and 1% Triton X-100) and lysed by gentle sonication. Then, the lysate was
356 centrifuged at 12,000×*g*, 4°C for 15 min. The supernatant was collected and mixed with a 50:50 slurry
357 of glutathione-Sepharose beads in chilled PBS lysis buffer. The bead-cell mix was incubated at 4°C to
358 trap proteins on the beads. Then, the beads were washed with ice-cold PBS containing protease
359 inhibitors and loaded into a disposable chromatography column. Trapped GST-GFP-NLS was eluted
360 with ice-cold 50 mM Tris-HCl (pH 8.0) containing 20 mM reduced glutathione. Molecular weight of
361 the collected GST-GFP-NLS was confirmed by polyacrylamide gel electrophoresis. Throughout this
362 study, GST-GFP-NLS is referred to as 'GFP-NLS'.

363

364 **Intra-GUV nuclear assembly protocol**

365 To achieve reconstitution of cell nuclei in GUVs, we designed an experimental protocol as illustrated
366 in Fig. 1. Briefly, the protocol consists of three steps: 1) preparation of *Xenopus* interphase egg extract

367 supplemented with sperm chromatin, 2) formation of GUVs encapsulating the sperm chromatin-added
368 interphase egg extract by the inverted emulsion method, and 3) induction of nuclear assembly reactions
369 in the formed GUVs. In the first step, the sperm chromatin-added egg extract was prepared for *in vitro*
370 nuclear assembly reactions [15-17] as depicted in Fig. 1a. In the second step, GUVs encapsulating the
371 egg extract were formed at a chilled temperature by the inverted emulsion method [25] with two
372 modifications to the conventional protocol: i) implementing prolonged waiting time and ii) adding
373 chloroform into lipid-dispersed oil to facilitate the formation of GUVs encapsulating the egg extract
374 as illustrated in Fig. 1b. In the third step, the GUVs were incubated at 22-23ºC to initiate the assembly
375 of interphase nuclei within them as depicted in Fig. 1c.

376

377 **Formation of GUVs encapsulating *Xenopus* interphase egg extract**

378 The lipid-dispersed oil (lipid-oil) was prepared using the following procedure. 1-palmitoyl-2-oleoyl-
379 glycero-3-phosphocholine (POPC) at a concentration of 25 mg $mL^{-1}$ in chloroform, and 1,2-dioleoyl-
380 sn-glycero-3-phosphoethanolamine-N-(lissamine rhodamine B sulfonyl) ammonium salt (RhPE) at 1
381 mg $mL^{-1}$ in chloroform, both purchased from Avanti Polar Lipids (USA), were taken to a disposable
382 glass bottle with a screw top (Laboran, As One, Japan). The chloroform was evaporated in a desiccator
383 for 30-60 min using a vacuum pump. Mineral oil (M5904, Sigma Aldrich) was then immediately added
384 to the bottle. The final composition of the lipid-oil was 2.5 mM of POPC with 0.1% (mole percent)
385 RhPE in mineral oil. For the GUVs in immunostaining experiment, RhPE was not added. Subsequently,
386 chloroform ($\Delta$ = 0/5/10% depending on the experimental condition) was added using a disposable
387 pipette. The screw top was tightly closed, and a strip of adhesive tape was attached to ensure sealing.
388 The lipid-oil was sonicated at 60°C for 1 h and stored at room temperature until use. In all experiments,
389 the lipid-oil was consumed within a week after preparation. The lipid-oil was sonicated at 60°C for 1
390 h before each use.

391

392 GUVs were formed by the inverted emulsion method [25] according to the following protocol. First,
393 two 1.5 mL disposable tubes and a 2.0 mL disposable centrifuge tube were prepared. 150 μL of egg
394 lysis buffer (250 mM sucrose, 10 mM HEPES-KOH pH 7.7, 50 mM KCl, 2.5 mM $MgCl_2$, and 1 mM
395 dithiothreitol) [49] was added to each of the 1.5 mL tubes, and 1.0 mL of lipid-oil was added to the 2.0
396 mL centrifuge tube. All tubes were then placed on ice. Next, 25 μL of frozen *Xenopus* interphase egg
397 extract stored at -80°C was thawed on ice. Subsequently, 0.5 μL of energy mix (50 mM ATP, 50 mM
398 $MgCl_2$, 10 mM phosphocreatine, 100 μg $mL^{-1}$ creatine kinase, pH 7.5 adjusted with NaOH) and 0.5
399 μL of GFP-NLS (3.4 mg $mL^{-1}$ for experiments in Figs. 2, 3a top, 4d-f and Supplementary Figs. 3-4, 7-
400 8, 13-14, 16-17 and 11.1 mg $mL^{-1}$ for experiments in Figs. 3b, 4b-c and Supplementary Figs. 1, 9-12,
401 15) for NLS(+) condition or GFP (7.7 mg $mL^{-1}$ for experiments in Figs. 3a bottom and 3b bottom, 4b-
402 c, Supplementary Figs. 8, 12; purchased from Chromotek, Germany) for NLS(-) condition were added
403 to the thawed egg extract. This mixture was briefly vortexed and spun down. Subsequently, 0.5 μL of
404 thawed *Xenopus* sperm chromatin was added on ice and the extract was mixed by gently pipetting four
405 times. 25 μL of this extract mix was then added to 1 mL of chilled lipid-oil in the 2.0 mL centrifuge
406 tube. Additionally, 150 μL of lipid-oil was layered on top of the egg lysis buffer in the two 1.5 mL
407 tubes on ice. These three tubes were incubated on ice for the designated duration of waiting time ($\tau$ =
408 0/60/120 min).

409

410 Following the incubation of the oil-water interface on ice, the mixture of lipid-oil and the egg extract
411 was vortexed for 1 min at 3,200 RPM using a Vortex-Genie 2 (Scientific Industries, Inc.). 500 μL of
412 the vortexed mixture of the egg extract in lipid-oil was immediately layered on top of each of the
413 chilled lipid-oil layers in the 1.5 mL tubes. The two 1.5 mL tubes were centrifuged at 9,000×*g*, 4°C for
414 30 min. During this centrifugation, a new 1.5 mL tube filled with 1 mL of the egg lysis buffer was

415 prepared and chilled on ice. Subsequently, the centrifuged tubes were collected, and the formed GUVs
416 in the bottom pellet were transferred into 1 mL of the chilled egg lysis buffer in a 1.5 mL tube by
417 piercing the side wall of the pellet in the tube with a syringe needle and applying air pressure from the
418 open top of the tube using an index finger. Finally, the collected GUVs dispersed in the egg lysis buffer
419 were vortexed briefly and kept on ice until further experiment.

420

421 **Induction of nuclear assembly reactions**

422 Nuclear assembly in GUVs encapsulating sperm chromatin-added *Xenopus* interphase egg extract was
423 conducted by incubating the formed GUVs dispersed in the egg lysis buffer either on a tube rack at
424 23°C or on a block incubator set at 22°C for 90 min. Note that all GUVs encapsulating the egg extract
425 formed by our inverted emulsion method were incubated for nuclear assembly reactions before
426 fluorescence staining and microscopy.

427

428 Nuclear assembly under bulk condition was performed by the following procedure. Firstly, the frozen
429 egg extract, energy mix, GFP-NLS, and sperm chromatin were thawed on ice. Subsequently, 1 μL of
430 energy mix and 1 μL of GFP-NLS were added to 50 μL of the thawed egg extract in a 0.5 mL tube.
431 This egg extract was vortexed briefly, spun down, and placed on ice immediately. Then, 1 μL of sperm
432 chromatin was added to the egg extract. This egg extract was gently pipetted four times, spun down
433 briefly, and placed back on ice immediately. The 0.5 mL tube containing the extract mix was then
434 placed on a block incubator set at 22°C and incubated for 90 min to induce nuclear assembly reactions
435 in the bulk egg extract.

436

437 **Fluorescence staining and preparation of glass slide samples for microscopy**

438 GUVs encapsulating the egg extract dispersed in the egg lysis buffer were centrifuged at 200×*g* for 5
439 min at room temperature. The supernatant was carefully removed, and the sample volume was reduced
440 to 140 μL. For fluorescence staining of DNA, 0.14 μL of 5 mM SYTO 41 (Thermo Fisher Scientific)
441 was added to the sample by a 1,000× dilution. Subsequently, the stained GUVs were briefly vortexed
442 and transferred into the open well of a Frame-Seal chamber (SLF1201, Bio-Rad) attached to a BSA-
443 coated glass slide. The chamber was immediately sealed with a No.1 glass coverslip coated with BSA.
444 To facilitate microscopy, the glass slide sample was immediately inverted so that the No.1 coverslip
445 faced downward, allowing the GUVs to settle towards the bottom surface prior to microscopy.

446

447 **Microscopy**

448 An inverted microscope (IX71, Olympus) equipped with an oil immersion objective (PlanApoN 60×,
449 1.45 NA, Olympus), fluorescence filters (460/80 nm, 520/35 nm, and 617/73 nm Bright-Line single-
450 bandpass filters, Semrock, USA), a laser combiner (405/488/561 nm, ALC5000, Andor Technology,
451 UK), a spinning disk confocal unit (CSU-X1, Yokogawa, Japan), and an EM-CCD camera (iXon X3,
452 Andor Technology, UK) was used for all micrographs in the main text of this paper. Imaging sequences
453 were programmed and executed using iQ2 software (Andor Technology, UK).

454

455 **Immunostaining of nuclear pore complexes on nuclear membranes**

456 Immunostaining of nuclear pore complexes (NPCs) on the nuclei formed in the bulk form of the egg
457 extract and in GUVs encapsulating the egg extract was conducted as follows.

458

459 For fixing nuclei formed in bulk form of the egg extract, 50 μL of the nuclei-containing egg extract
460 was first mixed with 150 μL of the egg lysis buffer and pipetted gently. 200 μL of fixation solution

461 (4% glutaraldehyde in 80 mM KCl and 10 mM Tris-HCl pH 7.7) was added, and the tube was
462 immediately placed on ice and incubated for 1 h. After the incubation, the fixed nuclei were transferred
463 to a 1.5 mL tube filled with 1 mL of quenching solution (10 mM Tris-HCl pH 7.7, 250 mM sucrose,
464 50 mM KCl, 1% BSA) on ice. The sample was centrifuged at 200×*g*, 4°C for 5 min, and the supernatant
465 was gently removed. The sample was then centrifuged again, and the supernatant was removed down
466 to 100 μL. To stain NPCs on the membrane of the fixed nuclei, 1 μL of 0.5 mg $mL^{-1}$ mAb414-AF594
467 was added and gently mixed by pipetting. The fixed nuclei with mAb414-AF594 were incubated on
468 ice overnight. On the next day, the sample was centrifuged at 200×*g*, 4°C for 5 min. The supernatant
469 was removed down to 100 μL, and 0.1 μL of 5 mM SYTO 41 was added for DNA staining. The entire
470 volume of the immunostained nuclei was enclosed in a Frame-Seal chamber between a No.1 glass
471 coverslip and a glass slide, both of which were coated with BSA.

472

473 The fixation of nuclei formed in GUVs encapsulating the egg extract was performed in the following
474 procedure. The GUVs were centrifuged at 200×*g,* 4ºC for 5 min, and the supernatant was removed
475 down to 100 μL. The tube containing the GUVs was placed on ice, and 100 μL of the fixation solution
476 was added. After 1 h of incubation on ice, the fixed GUVs were mixed with 1 mL of quenching solution
477 and centrifuged at 200×*g* for 5 min at 4ºC. The supernatant was removed, and the volume was reduced
478 to 100 μL. The quenching and washing of the fixed GUVs were repeated once, and the sample volume
479 was adjusted to 100 μL. The fixed GUVs with NPC-antibodies were then incubated on ice overnight.
480 The following day, the sample was centrifuged at 200×*g*, 4ºC for 5 min, and the supernatant was
481 reduced to 140 μL. 0.14 μL of 5 mM SYTO 41 was added for DNA staining, and the immunostained
482 GUVs were enclosed in a Frame-Seal chamber between a No.1 glass coverslip and a glass slide, both
483 of which were coated with BSA.

484

485 **Image segmentation of GUVs**

486 Image segmentation of GUVs on acquired micrographs was performed using *cellpose 2.0* [50,51]
487 implemented in Python. The envelopes of GUVs were primarily segmented using a built-in model
488 ('CP'), and the quality of the segments was manually inspected and corrected on the graphical user
489 interface (GUI) of *cellpose 2.0*.

490

491 **Number, internal GFP intensity, and diameter of GUVs**

492 The analysis of GUV fluorescence using above generated segment masks was performed in MATLAB.
493 The number of GUVs was determined by computing the number of segments. The mean GFP intensity
494 in the GUVs, denoted as $I_{\mathrm{GFP}}$, was computed by extracting intensity values in the GFP channel using
495 the segmentation mask and taking their mean. The diameter of the GUVs was defined as the reduced
496 diameter of each circle having a corresponding area of individual segments. To determine the mean
497 GFP intensity in the background of each micrograph, three arbitrary rectangular regions with at least
498 1,056 pixels were carefully selected in the background of each micrograph. The corresponding mean
499 GFP fluorescence intensity was computed for each rectangular region, and the average of the three
500 means was calculated. The threshold of GFP encapsulation in Supplementary Figs. 4 and 17 was
501 defined by mean + 3SD of the mean GFP intensity in each background.

502

503 **Exclusion of GUVs containing aggregated GFP**

504 GUVs containing aggregated GFP were manually excluded from the dataset used to compute the
505 proportion of GUVs encapsulating the GFP-dispersed egg extract in the observed GUVs (Fig. 2c and
506 Supplementary Fig. 3). This exclusion aimed to mitigate artifacts in the computed proportion arising
507 from GFP aggregation in three-dimensional space. This issue was observed in all micrographs acquired

508 after completing the entire protocol of nuclear assembly in GUVs (Fig. 1). Since the GUVs in the
509 micrographs of Fig. 2 had already undergone 23ºC incubation for nuclear assembly reactions, several
510 GUVs in the acquired micrographs exhibited positive indications of nuclear import by GFP-NLS
511 within them. Theoretically, the mean GFP intensity computed from a confocal micrograph of such
512 GUVs with aggregated GFP always yielded a higher mean GFP intensity than a confocal micrograph
513 of GUVs without GFP aggregation even if the same amount of GFP was encapsulated. Consequently,
514 the mean GFP intensity of the GUVs containing the aggregation did not precisely reflect the
515 concentration of GFP encapsulated in the GUV. Because the purpose of the analysis in Fig. 2c was to
516 evaluate GFP encapsulation in the GUVs, we considered the inclusion of data from GUVs carrying
517 such aggregated GFP inadequate and excluded the GUVs from this specific analysis in Fig. 2c and
518 Supplementary Fig. 3. The same parameter computed from data including the GUVs containing
519 aggregated GFP is shown in Supplementary Fig. 16. Additionally, raw GFP intensity values in the
520 GUV lumen and the background of these GUVs are plotted in Supplementary Fig. 17. Comparisons
521 between plots excluding the GUVs containing aggregated GFP (Fig. 2c and Supplementary Figs. 3-4)
522 and those including them (Supplementary Figs. 16-17) indicate only minor changes.

523

524 **Definition and identification of NLCs in GUVs**

525 To differentiate between C1 compartments (Fig. 4a) containing a significantly high level of GFP-NLS
526 from those with a lower level, we set a threshold for the GFP intensity ratio, as indicated by the dashed
527 line in Fig. 4c. This threshold was determined as the mean + 3SD of the GFP intensity ratio under
528 NLS(-) conditions (dashed line in Fig. 4c). We used this threshold to interpret accumulation of GFP-
529 NLS in C1 compartment: if the ratio exceeded the threshold, it indicated GFP-NLS accumulation.
530 Utilising this threshold, we defined a 'nucleus-like compartment' (NLC) as a C1 compartment with a
531 GFP intensity ratio higher than the threshold.

532

533 To identify NLCs in GUVs, GUVs containing dense DNA (C1 compartment in Fig. 4a) were initially
534 identified in micrographs through manual inspection. Subsequently, the envelopes of the GUVs and
535 their internal C1 compartments were manually segmented in RhPE and SYTO41 channels using the
536 interactive *drawfreehand* function in MATLAB. Mean intensity values of SYTO 41 signals in the C1
537 and C2 compartments were then computed using the segment masks. Similarly, mean GFP intensities
538 in the C1 and C2 compartments were computed using the same segment masks. Next, the ratio of mean
539 intensities in the C1 and C2 compartments was computed for both the SYTO 41 and GFP channels.
540 The threshold for the GFP intensity ratio was determined based on the above definition (computed
541 threshold: ~1.5). Furthermore, to ensure the encapsulation of DNA and GFP-NLS in the NLCs, the
542 mean fluorescence intensity of both SYTO 41 and GFP in the background (Supplementary Fig. 12)
543 was calculated. This computation was done by extracting three arbitrary rectangular regions from the
544 background, each containing at least 1,517 pixels. The mean fluorescence intensity of each region was
545 computed, and the average of these three mean values was taken.

546

547 **Proportion and size of GUVs containing an NLC**

548 All confocal micrographs of GUVs encapsulating the egg extract after 90 min incubation at 22°C were
549 manually examined, and NLCs were identified following their definition. The number of identified
550 NLCs at each waiting time and chloroform condition was divided by the total number of GUVs found
551 in all micrographs inspected for NLCs. For computing the total number of GUVs in the micrographs
552 inspected for NLC formation, image segmentation using built-in 'CP' model of *cellpose 2.0* in Python
553 was performed. While raw segments generated with this 'CP' model often require correction of their
554 shapes to increase the reliability in successive computation of parameters such as fluorescence
555 intensity using the segments, the number of GUVs is generally accurate. Thus, we only checked

556 whether unwanted artifacts (segments) were included in the segment masks or not by manual
557 inspection.

558

559 The diameter of GUVs containing an NLC and that of GUVs not containing an NLC at $\tau$ = 120 min
560 and $\Delta$ = 10% shown in Fig. 4d were computed in the following procedure. Since accurate manual
561 image segmentation of GUVs containing an NLC was conducted when NLCs were identified, only the
562 segments of GUVs without NLC in the same number were collected from two micrographs randomly.
563 Using the segments of these GUVs, the reduced diameter was computed from their segment area.

564

565 **Statistical analysis**

566 In the statistical analysis depicted in Fig. 2b-c and 2e, as well as Supplementary Figs. 2-3, 5-6, and 16,
567 we conducted one-way ANOVA followed by *post-hoc* Tukey-Kramer multiple comparison tests,
568 focusing either on the duration of waiting time or the added volume of chloroform. For the statistical
569 analysis conducted in Fig. 4b-c, we first confirmed the normality of each dataset using the Lilliefors
570 test, followed by a two-sample t-test. In the statistical analysis shown in Fig. 4d and 4g, and
571 Supplementary Fig. 13, we employed the Wilcoxon rank sum test. For the statistical analysis in Fig.
572 4e, a Kruskal-Wallis test followed by a *post-hoc* multiple comparison test with Bonferroni's correction
573 was performed. For all analyses, resultant $p$-values were rounded to the first significant digit and
574 annotated using the conventional method: 'n.s.' (not significant) for $p > 0.05$, '*' for $p \leq 0.05$, '**' for
575 $p \leq 0.01$, and '***' for $p \leq 0.001$. The details of all statistical analyses are summarised in
576 Supplementary Tables 1-16.

577

578 **Data availability**

Data supporting the results of this study are available from the corresponding authors upon request.

**Code availability**

The code used for the simulation is available from the corresponding authors upon request.

**References**


[1] Jia, H., & Schwille, P. Bottom-up synthetic biology: reconstitution in space and time. *Current opinion in biotechnology*, **60** 179-187 (2019).

[2] Simmel, F. C. Synthetic organelles. *Emerging Topics in Life Sciences* **3**(5), 587-595 (2019).

[3] Buddingh', B. C., & van Hest, J. C. Artificial cells: synthetic compartments with life-like functionality and adaptivity. *Accounts of chemical research* **50**(4), 769-777 (2017).

[4] Gaut, N. J., & Adamala, K. P. Reconstituting natural cell elements in synthetic cells. *Advanced Biology* **5**(3), 2000188 (2021).

[5] Elani, Y. Interfacing living and synthetic cells as an emerging frontier in synthetic biology. *Angewandte Chemie* **133**(11), 5662-5671 (2021).

[6] Lee, K. Y., Park, S. J., Lee, K. A., Kim, S. H., Kim, H., Meroz, Y., ... & Shin, K. Photosynthetic artificial organelles sustain and control ATP-dependent reactions in a protocellular system. *Nature biotechnology* **36**(6), 530-535 (2018).

[7] Berhanu, S., Ueda, T., & Kuruma, Y. Artificial photosynthetic cell producing energy for protein synthesis. *Nature communications* **10**(1), 1325 (2019).

[8] Kumar, B. P., Fothergill, J., Bretherton, J., Tian, L., Patil, A. J., Davis, S. A., & Mann, S. Chloroplast-containing coacervate micro-droplets as a step towards photosynthetically active membrane-free protocells. *Chemical communications* **54**(29), 3594-3597 (2018).

602 [9] Otrin, L., Marušič, N., Bednarz, C., Vidakovic-Koch, T., Lieberwirth, I., Landfester, K., &
603 Sundmacher, K. Toward artificial mitochondrion: mimicking oxidative phosphorylation in
604 polymer and hybrid membranes. *Nano letters* **17**(11), 6816-6821 (2017).
605 [10] Marušič, N., Otrin, L., Zhao, Z., Lira, R. B., Kyrilis, F. L., Hamdi, F., ... & Dimova, R.
606 Constructing artificial respiratory chain in polymer compartments: Insights into the interplay
607 between $bo_3$ oxidase and the membrane. *Proceedings of the National Academy of Sciences* **117**(26),
608 15006-15017 (2020).
609 [11] Westensee, I. N., Brodszkij, E., Qian, X., Marcelino, T. F., Lefkimmiatis, K., & Städler, B.
610 Mitochondria encapsulation in hydrogel-based artificial cells as ATP producing subunits. *Small*
611 **17**(24), 2007959 (2021).
612 [12] Deng, N. N., Yelleswarapu, M., Zheng, L., & Huck, W. T. Microfluidic assembly of
613 monodisperse vesosomes as artificial cell models. *Journal of the American Chemical Society*
614 **139**(2), 587-590 (2017).
615 [13] Aufinger, L., & Simmel, F. C. Artificial gel-based organelles for spatial organization of cell-
616 free gene expression reactions. *Angewandte Chemie International Edition* **57**(52), 17245-17248
617 (2018).
618 [14] Göpfrich, K., Platzman, I., & Spatz, J. P. Mastering complexity: towards bottom-up
619 construction of multifunctional eukaryotic synthetic cells. *Trends in biotechnology* **36**(9), 938-951
620 (2018).
621 [15] Lohka, M. J., & Masui, Y. Formation *in vitro* of sperm pronuclei and mitotic chromosomes
622 induced by amphibian ooplasmic components. *Science* **220**(4598), 719-721 (1983).
623 [16] Newmeyer, D. D., Lucocq, J. M., Bürglin, T. R., & De Robertis, E. M. Assembly *in vitro* of
624 nuclei active in nuclear protein transport: ATP is required for nucleoplasmin accumulation. *The*
625 *EMBO journal* **5**(3), 501-510 (1986).

[17] Newport, J. Nuclear reconstitution *in vitro*: stages of assembly around protein-free DNA. *Cell* **48**(2), 205-217 (1987).

[18] Hara, Y., & Merten, C. A. Dynein-based accumulation of membranes regulates nuclear expansion in *Xenopus laevis* egg extracts. *Developmental cell* **33**(5), 562-575 (2015).

[19] Bisht, J., LeValley, P., Noren, B., McBride, R., Kharkar, P., Kloxin, A., ... & Oakey, J. Light-inducible activation of cell cycle progression in *Xenopus* egg extracts under microfluidic confinement. *Lab on a Chip* **19**(20), 3499-3511 (2019).

[20] Good, M. C. Encapsulation of *Xenopus* egg and embryo extract spindle assembly reactions in synthetic cell-like compartments with tunable size. *The Mitotic Spindle: Methods and Protocols* 87-108 (2016).

[21] Guan, Y., Li, Z., Wang, S., Barnes, P. M., Liu, X., Xu, H., ... & Yang, Q. A robust and tunable mitotic oscillator in artificial cells. *Elife* **7**, e33549 (2018).

[22] Guan, Y., Wang, S., Jin, M., Xu, H., & Yang, Q. Reconstitution of cell-cycle oscillations in microemulsions of cell-free *Xenopus* egg extracts. *JoVE (Journal of Visualized Experiments)* (**139**), e58240 (2018).

[23] Bermudez, J. G., Chen, H., Einstein, L. C., & Good, M. C. Probing the biology of cell boundary conditions through confinement of *Xenopus* cell-free cytoplasmic extracts. genesis **55**(1-2), e23013 (2017).

[24] Chiba, M., Miyazaki, M., & Ishiwata, S. I. Quantitative analysis of the lamellarity of giant liposomes prepared by the inverted emulsion method. *Biophysical journal*, **107**(2), 346-354 (2014).

[25] Pautot, S., Frisken, B. J., & Weitz, D. A. Production of unilamellar vesicles using an inverted emulsion. *Langmuir* **19**(7), 2870-2879 (2003).

[26] Claudet, C., In, M., & Massiera, G. Method to disperse lipids as aggregates in oil for bilayers production. *The European Physical Journal E* **39**, 1-6 (2016).

[27] Dilsaver, M. R., Chen, P., Thompson, T. A., Reusser, T., Mukherjee, R. N., Oakey, J., & Levy, D. L. Emerin induces nuclear breakage in *Xenopus* extract and early embryos. *Molecular Biology of the Cell* **29**(26), 3155-3167 (2018).

[28] Nord, M. S., Bernis, C., Carmona, S., Garland, D. C., Travesa, A., & Forbes, D. J. Exportins can inhibit major mitotic assembly events *in vitro*: membrane fusion, nuclear pore formation, and spindle assembly. *Nucleus* **11**(1), 178-193 (2020).

[29] Van de Cauter, L., Fanalista, F., Van Buren, L., De Franceschi, N., Godino, E., Bouw, S., ... & Ganzinger, K. A. Optimized cDICE for efficient reconstitution of biological systems in giant unilamellar vesicles. *ACS Synthetic Biology* **10**(7), 1690-1702 (2021).

[30] Shimane, Y., & Kuruma, Y. Rapid and facile preparation of giant vesicles by the droplet transfer method for artificial cell construction. *Frontiers in Bioengineering and Biotechnology* **10**, 873854 (2022).

[31] Nishimura, K., Matsuura, T., Nishimura, K., Sunami, T., Suzuki, H., & Yomo, T. Cell-free protein synthesis inside giant unilamellar vesicles analyzed by flow cytometry. *Langmuir* **28**(22), 8426-8432 (2012).

[32] Walczak, M., Brady, R. A., Mancini, L., Contini, C., Rubio-Sánchez, R., Kaufhold, W. T., ... & Di Michele, L. Responsive core-shell DNA particles trigger lipid-membrane disruption and bacteria entrapment. *Nature Communications* **12**(1), 4743 (2021).

[33] Loiseau, E., Schneider, J. A., Keber, F. C., Pelzl, C., Massiera, G., Salbreux, G., & Bausch, A. R. Shape remodeling and blebbing of active cytoskeletal vesicles. *Science Advances* **2**(4), e1500465 (2016).

[34] Litschel, T., Ramm, B., Maas, R., Heymann, M., & Schwille, P. Beating vesicles: encapsulated protein oscillations cause dynamic membrane deformations. *Angewandte Chemie International Edition* **57**(50), 16286-16290 (2018).

674 [35] Litschel, T., Kelley, C. F., Holz, D., Adeli Koudehi, M., Vogel, S. K., Burbaum, L., ... &
675 Schwille, P. Reconstitution of contractile actomyosin rings in vesicles. *Nature communications*
676 **12**(1), 2254 (2021).
677 [36] Baldauf, L., Frey, F., Perez, M. A., Idema, T., & Koenderink, G. H. Branched actin cortices
678 reconstituted in vesicles sense membrane curvature. *Biophysical journal* **122**(11), 2311-2324
679 (2023).
680 [37] Hara, Y. Specialization of nuclear membrane in eukaryotes. *Journal of Cell Science* **133**(12),
681 jcs241869 (2020).
682 [38] Yandrapalli, N., Seemann, T., & Robinson, T. On-chip inverted emulsion method for fast giant
683 vesicle production, handling, and analysis. *Micromachines* **11**(3), 285 (2020).
684 [39] Moga, A., Yandrapalli, N., Dimova, R., & Robinson, T. Optimization of the inverted emulsion
685 method for high-yield production of biomimetic giant unilamellar vesicles. *ChemBioChem* **20**(20),
686 2674-2682 (2019).
687 [40] Sakamoto, R., Tanabe, M., Hiraiwa, T., Suzuki, K., Ishiwata, S. I., Maeda, Y. T., & Miyazaki,
688 M. Tug-of-war between actomyosin-driven antagonistic forces determines the positioning
689 symmetry in cell-sized confinement. *Nature communications* **11**(1), 3063 (2020).
690 [41] Murray, A. W., & Szostak, J. W. Construction of artificial chromosomes in yeast. *Nature*
691 **305**(5931), 189-193 (1983).
692 [42] Harrington, J. J., Bokkelen, G. V., Mays, R. W., Gustashaw, K., & Willard, H. F. Formation of
693 de novo centromeres and construction of first-generation human artificial microchromosomes.
694 *Nature genetics* **15**(4), 345-355 (1997).
695 [43] Gibson, D. G., Benders, G. A., Andrews-Pfannkoch, C., Denisova, E. A., Baden-Tillson, H.,
696 Zaveri, J., ... & Smith, H. O. Complete chemical synthesis, assembly, and cloning of a *Mycoplasma*
697 *genitalium* genome. *Science* **319**(5867), 1215-1220 (2008).

[44] Hutchison III, C. A., Chuang, R. Y., Noskov, V. N., Assad-Garcia, N., Deerinck, T. J., Ellisman, M. H., ... & Venter, J. C. Design and synthesis of a minimal bacterial genome. *Science* **351**(6280), aad6253 (2016).

[45] Saito, A. C., Ogura, T., Fujiwara, K., Murata, S., & Nomura, S. I. M. Introducing micrometer-sized artificial objects into live cells: A method for cell–giant unilamellar vesicle electrofusion. *PLoS One* **9**(9), e106853 (2014).

[46] Takamori, S., Cicuta, P., Takeuchi, S., & Di Michele, L. DNA-assisted selective electrofusion (DASE) of *Escherichia coli* and giant lipid vesicles. *Nanoscale* **14**(38), 14255-14267 (2022).

[47] Shintomi, K., & Hirano, T. A sister chromatid cohesion assay using *Xenopus* egg extracts. *Methods in Molecular Biology* **1515**, 3-21 (2017).

[48] Einarson, M. B., Pugacheva, E. N., & Orlinick, J. R. Preparation of GST fusion proteins. *Cold Spring Harbor Protocols* **2007**(4), pdb-prot4738 (2007).

[49] Cheng, X., & Ferrell Jr, J. E. Spontaneous emergence of cell-like organization in *Xenopus* egg extracts. *Science* **366**(6465), 631-637 (2019).

[50] Stringer, C., Wang, T., Michaelos, M., & Pachitariu, M. Cellpose: a generalist algorithm for cellular segmentation. *Nature methods* **18**(1), 100-106 (2021).

[51] Pachitariu, M., & Stringer, C. Cellpose 2.0: how to train your own model. *Nature methods* **19**(12), 1634-1641 (2022).

## Acknowledgements

We thank Dr Yuki Hara for kindly offering purified GFP-NLS and the corresponding plasmid. This study is partially supported by JST CREST (Grant number: JPMJCR18S5 to S.Takeuchi and M.O.) and JSPS KAKENHI (Grant numbers: JP22K15080 to S.Takamori, JP19H05755 and JP22H02551 to K.S.).

722

723 **Contributions**

724 All authors contributed the design of the research. S.Takamori conducted all experiments, with the
725 exception of the preparation of *Xenopus* egg extract and demembranated sperm chromatin, which were
726 performed by M.S. and K.S.. S.Takamori carried out all data analysis and drafted the initial manuscript.
727 All authors contributed to the interpretation of the data and editing of the manuscript.

728

729 **Corresponding author**

730 Correspondence to Shoji Takeuchi.

731

732 **Competing interests**

733 The authors declare no competing interests.

734

735 **Additional information**

736 **Supplementary information** The online version contains supplementary material available at URL.

737